Molecular Crystals and Liquid Crystals
Publication details, including instructions for authors and subscription information:
http://www.tandfonline.com/loi/gmcl16

Molecular Orientations and Optical Patterns of Rotating Nematics

He Gang [a] , Shu Changqing [a] & Lin Lei [b c d]

[a] Institute of Physics, Chinese Academy of Sciences, Beijing, China

[b] Department of Physics, City College, City University of New York, N. Y., 10031

[c] Department of Physics, Queensborough Community College, City University of New York, Bayside, N. Y., 11364

[d] Institute of Physics, Chinese Academy of Sciences, Beijing, China

Version of record first published: 17 Oct 2011.

To cite this article: He Gang , Shu Changqing & Lin Lei (1985): Molecular Orientations and Optical Patterns of Rotating Nematics, Molecular Crystals and Liquid Crystals, 124:1, 53-71

To link to this article: http://dx.doi.org/10.1080/00268948508079465

Mol. Cryst. Liq. Cryst., 1985, Vol. 124, pp. 53–71
0026-8941/85/1244–053/$20.00/0

Printed in the United States of America

Molecular Orientations and Optical Patterns of Rotating Nematics†

HE Gang and SHU Changqing

Institute of Physics, Chinese Academy of Sciences, Beijing, China

and

LIN Lei

Department of Physics, City College, City University of New York, N.Y. 10031,‡ and Department of Physics, Queensborough Community College, City University of New York, Bayside, N.Y. 11364, and Institute of Physics, Chinese Academy of Sciences, Beijing, China

(*Received October 15, 1984*)

The equation of motion of director for nematic liquid crystal flowing in the azimuthal direction with axial symmetry (as in e.g. torsional flow) is derived from the Ericksen-Leslie theory. When specialized to the case of homeotropic nematics in a circular cell, in the steady state, the two-dimensional equation may be simplified to a one-dimensional ordinary differential equation under the assumption that either the cell is thick (Model A) or the director angle varies very slowly with the dimensionless radial coordinate R (Model B). Both these two cases are analysed. For Model B, multiple solutions are found and discussed. Spatial distribution of the director is studied and the corresponding optical interference patterns of transmitted monochromatic light are calculated. When compared with experiments of Wahl and Fischer we found that the theoretical positions of the bright rings and the total number of bright rings lying within a radius of R are in agreement with experiments for $R < 10$ and $R < 130$, respectively.

In addition, the theoretical analysis of Wahl and Fischer which differs from ours is examined in detail and found to contain errors in its mathematical derivations. When these errors are properly corrected the domain of validity of Wahl and Fischer's theory is still only half that of ours. Also, the ratio of elastic constants deduced from their own experimental data using their theory is unreliable.

†Paper presented at the Tenth International Liquid Crystal Conference, York, United Kingdom, July 15–21, 1984.

‡Correspondence address.

I. INTRODUCTION

Homeotropic nematic liquid crystals undergoing torsional flow (in a circular cell) in the steady state was first investigated by Wahl and Fischer,[1,2] in both experiments and theory. The experiment was performed by rotating one glass disc with respect to the other and monochromatic light was transmitted vertically through two crossed polarizers. Alternative bright and dark rings are observed. Subsequently, this type of experiments were repeated with the addition of external electric fields[3-6] or magnetic fields.[7-9]

Presently, this type of torsional shear experiments has become one of the standard methods in measuring elastic constants and viscosities of nematics. Theoretical analysis related to the experimental situation was first provided by Wahl and Fischer[1] and has been used ever since. However, in this theory,[1] very strong assumptions are introduced; its consequences have been compared to experiments only indirectly; the domain of validity has not been analysed. Furthermore, there exists couple of errors in its mathematical derivations (see Section IV).

In view of its experimental importance and the existing deficiencies mentioned above, and as a first step in understanding solitons in rotating nematics,[10] in this paper, the experiments of Wahl and Fischer[1,2] will be reanalysed and a new theoretical analysis will be presented. In Section II, the director equation of motion of axially symmetric shearing nematic is derived from the Ericksen-Leslie theory.[11] Two special cases of one-dimensional models are analysed and numerical solutions are presented. In Section III, the optical interference patterns are calculated and compared directly with experiments. The results and theory of Reference 1 are analysed and discussed in respect to our theory in Section IV. A brief summary is given in Section V.

II. DIRECTOR EQUATION OF MOTION

For nematic rotating with angular velocity $\omega = \omega(z)$, the velocity is given by $v = v(r,z) = \omega(z)r$ (see Figure 1). For axially symmetric shear flow,

$$\mathbf{v} = (-v \sin\varphi, v\cos\varphi, 0) \tag{2.1}$$

where φ is the azimuthal angle and r the radial distance of the molecule. For small ω (as in the experiments of References of 1 and 2),

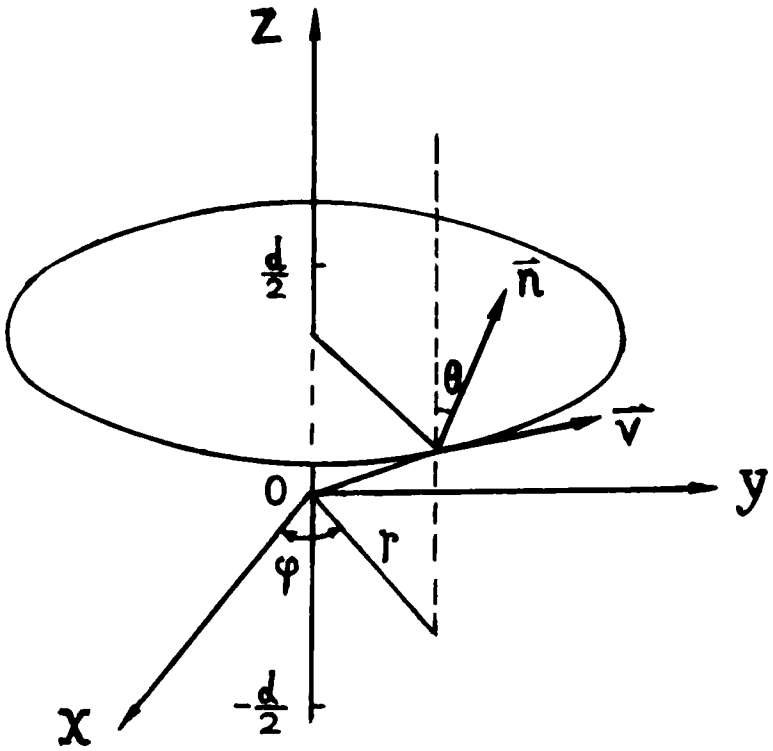

FIGURE 1. Velocity **v** and director **n** in a torsional shear flow. **v** is in the $\hat{\varphi}$ direction, **n** in the $(\hat{\varphi},\hat{z})$ plane.

it is reasonable to assume that the director **n** is in the $(\hat{\varphi}, \hat{z})$ plane, i.e.,

$$\mathbf{n} = (-\sin\theta \sin\varphi, \sin\theta \cos\varphi, \cos\theta) \tag{2.2}$$

where θ is the angle between **n** and $\hat{z}$.

Under the assumptions of Eq. (2.1) and (2.2), the director equation of motion as derived from the Ericksen-Leslie theory[11] becomes (see Appendix A of Reference 12 for details)

$$K_2 \frac{\partial^2\theta}{\partial r^2} + \frac{1}{r}(K_2 + K_3 \sin^2\theta)\frac{\partial\theta}{\partial r} + (K_1 \sin^2\theta + K_3 \cos^2\theta)\frac{\partial^2\theta}{\partial z^2}$$

$$+ \tfrac{1}{2}K_1 \sin 2\theta \left(\frac{\partial\theta}{\partial z}\right)^2 - \frac{\tfrac{1}{2}K_2}{r^2}\sin 2\theta - \frac{2(K_3 - K_2)}{r^2}\cos\theta \sin^3\theta \tag{2.3}$$

$$+ \tfrac{1}{2}s(z)r(\gamma_1 - \gamma_2 \cos 2\theta) - 2M\omega^2 \sin 2\theta = M\frac{\partial^2\theta}{\partial t^2} + \gamma_1 \frac{\partial\theta}{\partial t}$$

where $s(z) \equiv \partial\omega(z)/\partial z$. Note that M is the moment of inertia per unit volume, $K_i (i = 1,2,3)$ the elastic constants and γ_1, γ_2 the viscosities (the notations are those of Reference 13). The absence of φ in Eq. (2.3) is a natural consequence of the axial symmetry of the problem. Since $M \sim 10^{-12}$ gm cm^{-1}, for our purpose, we may set $M = 0$ in Eq. (2.3) and work, in the steady state, with the equation,

$$K_2 \frac{\partial^2\theta}{\partial r^2} + \frac{1}{r}(K_2 + K_3 \sin^2\theta)\frac{\partial\theta}{\partial r} + (K_1 \sin^2\theta + K_3 \cos^2\theta)\frac{\partial^2\theta}{\partial z^2}$$

$$+ \tfrac{1}{2}K_1 \sin 2\theta \left(\frac{\partial\theta}{\partial z}\right)^2 - \tfrac{1}{2}\frac{K_2}{r^2}\sin 2\theta - \frac{2(K_3 - K_2)}{r^2}\cos\theta \sin^3\theta \qquad (2.4)$$

$$+ \tfrac{1}{2}s(z)r(\gamma_1 - \gamma_2 \cos 2\theta) = 0$$

Let us assume that the nematic is sandwiched between $z = \pm d/2$ and undergoes torsional flow with $\omega(d/2) = \omega_0$, $\omega(-d/2) = 0$ where ω_0 (denoted by ω in Reference 1) is a constant. For uniform torsional shear such that $s(z) = \omega_0/d$ = constant, Eq. (2.4) is decoupled from the center of mass degree of freedom and may be solved independently.

Defining

$$R \equiv \lambda r,\ \lambda \equiv [\omega_0|\gamma_2|/(2K_3 d)]^{1/3},\ \xi \equiv 2z/d,$$

$$c \equiv K_1/K_3,\ b \equiv K_2/K_3,\ \gamma \equiv \gamma_1/|\gamma_2|,\ D \equiv \lambda d/2$$

Eq. (2.4) in the dimensionless form becomes

$$b\frac{\partial^2\theta}{\partial R^2} + \frac{1}{D^2}(c \sin^2\theta + \cos^2\theta)\frac{\partial^2\theta}{\partial\xi^2} + \frac{c}{2D^2}\sin 2\theta \left(\frac{\partial\theta}{\partial\xi}\right)^2$$

$$+ \frac{1}{R}(b + \sin^2\theta)\frac{\partial\theta}{\partial R} - \frac{b}{2R^2}\sin 2\theta - \frac{2(1-b)}{R^2}\sin^3\theta \cos\theta \qquad (2.5)$$

$$+ R(\gamma + \cos 2\theta) = 0$$

For homeotropic nematic, the boundary conditions are

$$\theta(R,\xi)\Big|_{\xi=\pm 1} = 0,\ \theta(R,\xi)\Big|_{R=0} = 0,\ \frac{\partial\theta}{\partial R}(R,\xi)\Big|_{R=0} = \theta^*(\xi) \qquad (2.6)$$

where θ^* can be inferred from the experiments and is not known a priori. For planar nematics, the two zeros on the first two equations in Eq. (2.6) is replaced by $\pi/2$.

It is easy to see that the two-dimensional equation (2.5) does not possess spatial uniform solutions. Equation (2.5) is symmetrical with respect to $\xi \rightarrow -\xi$ and is valid for both homeotropic and planar conditions. In Eq. (2.5), D is a material parameter. When K_i, γ_1 and γ_2 are given for a material, D is determined by the combination of ω_0 and d.

Equations (2.5) and (2.6) will constitute the basis of discussion in the rest of this paper. As shown below, in special cases, it is possible to reduce Eq. (2.5) to a one-dimensional equation.

Model A: $\partial\theta/\partial\xi = \partial^2\theta/\partial\xi^2 = 0$

In the case of large d such that the boundary effects may be ignored we may set $\partial\theta/\partial\xi = \partial^2\theta/\partial\xi^2 = 0$ in Eq. (2.5) which, under the one-constant approximation ($K_1 = K_2 = K_3 \equiv K$), simplifies to

$$\frac{d^2\theta}{d\rho^2} + \frac{1}{3\rho}(3 + 2\sin^2\theta)\frac{d\theta}{d\rho} - \frac{2}{9}\frac{\sin 2\theta}{\rho^2} + (\gamma + \cos 2\theta) = 0 \quad (2.7)$$

where $\rho \equiv (2/3)R^{3/2}$.

For $\rho << 1$ (i.e. near the center of the cell), θ is very small and may be expanded in a series of ρ. When Eq. (2.7) is then linearized in θ we obtain[12]

$$\theta \simeq \frac{9}{32}(\gamma + 1)\rho^2$$

For $\rho >> 1$, the ρ^{-2} term in Eq. (2.7) may be ignored resulting in

$$\frac{d^2\theta}{d\rho^2} + \frac{1}{3\rho}(3 + 2\sin^2\theta)\frac{d\theta}{d\rho} + \frac{dV}{d\theta} = 0 \quad (2.8)$$

where

$$V \equiv \gamma\theta + \tfrac{1}{2}\sin 2\theta \quad (2.9)$$

Equation (2.9) describes the damped motion of a particle of unit mass in the potential V (taking ρ as the "time" variable). The variation

of V with θ is depicted in Figure 2 (for $\gamma = 0.96$). In Figure 2, $\theta_0 = -\frac{1}{2}\cos^{-1}(-\gamma)$, $\theta_1 = -\pi - \theta_0$ and $V(\theta_0) < V(\theta_1) < V(0)$. For MBBA at room temperature, one has[14] $\gamma = 0.96$ and $V(\theta_1) - V(\theta_0) << V(0) - V(\theta_0)$. The damping term in Eq. (2.9) decreases with ρ increasing. When the particle starts its downward motion at $\theta = 0$ at $\rho = 0$ (in the homeotropic case), this damping term is not strong enough to stop the particle at the valley at $\theta = \theta_0$. The particle in fact moves over the hilltop at $\theta = \theta_1$ and moves faster and faster all the way down the hill, i.e., θ decreases without limit as ρ increases. This result of θ vs. ρ remains true even if the one-constant approximation in Eq. (2.7) is lifted. Numerical results (not shown here) have been performed by us.

In the experiments of Wahl and Fischer,[1,2] since the spacing between the observed dark rings is relatively large for large ρ, θ is expected to change much slowly for ρ large. This is at odds with the above θ vs. ρ resulting from the neglect of ξ-dependence in Eq. (2.5). In fact, the boundary effect in the experiments[1,2] are estimated[12] to be very strong and the ξ-dependence of θ is important (see also

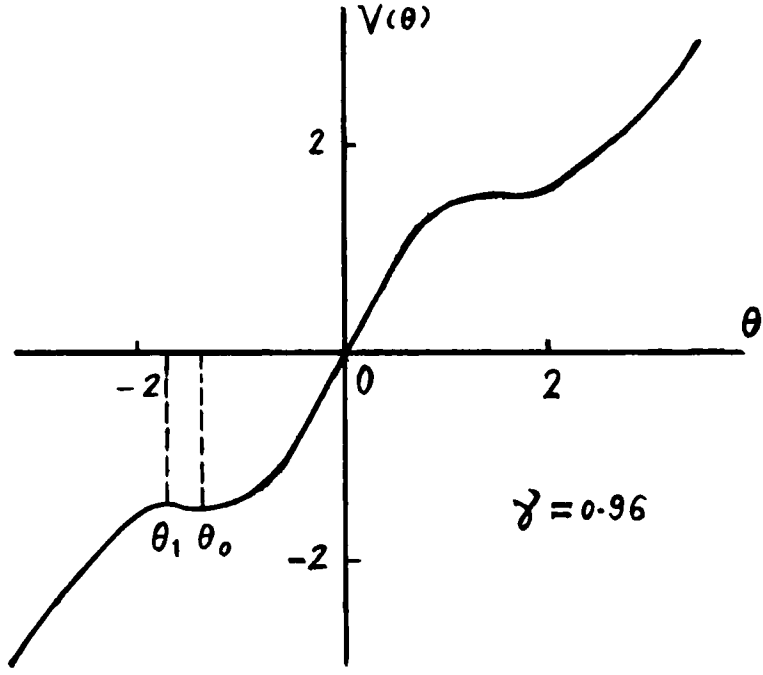

FIGURE 2. Variation of $V(\theta)$ with θ. $\gamma = 0.96$.

References 3 and 14). The basic approximation of a thick cell underlying Eq. (2.7) is inapplicable in the experimental situations of References 1 and 2. We therefore consider another type of approximation in the following.

Model B: $\partial\theta/\partial R = \partial^2\theta/\partial R^2 = 0$

When the ξ-dependence is strong the gradient terms of ξ in Eq. (2.5) cannot be ignored. In the case that θ varies slowly with R one may set $\partial\theta/\partial R = \partial^2\theta/\partial R^2 = 0$ in Eq. (2.5) and obtains

$$\frac{1}{D^2}(c\sin^2\theta + \cos^2\theta)\frac{d^2\theta}{d\xi^2} + \frac{c}{2D^2}\sin 2\theta\left(\frac{d\theta}{d\xi}\right)^2 - \frac{b}{2R^2}\sin 2\theta - \frac{2(1-b)}{R^2}\sin^3\theta\cos\theta + R(\gamma + \cos 2\theta) = 0 \quad (2.10)$$

Multiple solutions

For a qualitative understanding of the properties of Eq. (2.10) we apply the one-constant approximation and reduce Eq. (2.10) to

$$\frac{1}{D^2}\frac{d^2\theta}{d\xi^2} + \frac{1}{2D^2}\sin 2\theta\left(\frac{d\theta}{d\xi}\right)^2 - \frac{\sin 2\theta}{2R^2} + R(\gamma + \cos 2\theta) = 0 \quad (2.11)$$

For $R >> 1$, one may neglect the R^{-2} term in Eq. (2.11) and obtains

$$\frac{d^2\theta}{d\xi^2} + \tfrac{1}{2}\sin 2\theta\left(\frac{d\theta}{d\xi}\right)^2 + D^2R(\gamma + \cos 2\theta) = 0 \quad (2.12)$$

Let $\partial\theta/\partial\xi \equiv P$, $u \equiv P^2/2$, $R^* \equiv D^2R$. The first integration of Eq. (2.12) results in

$$u = R^* \exp(\tfrac{1}{2}\cos 2\theta)[C - F(\theta)] \quad (2.13)$$

where C is constant of integration and

$$F(\theta) \equiv \int_0^\theta d\theta(\gamma + \cos 2\theta)\exp(-\tfrac{1}{2}\cos 2\theta) \quad (2.14)$$

Because of the boundary condition in Eq. (2.6), if θ is a continuous

function of ξ then, by the mean-value theorem, there must exist a θ_m such that $d\theta/d\xi = 0$ at $\theta = \theta_m$. Consequently, $P = u = 0$ at $\theta = \theta_m$ and hence $C = F(\theta_m)$, leading to

$$u = R^* \exp\left(\tfrac{1}{2}\cos 2\theta\right) \int_{\theta}^{\theta_m} d\theta[exp(-\tfrac{1}{2}\cos 2\theta)(\gamma + \cos 2\theta)] \quad (2.15)$$

The curve $F(\theta)$ may be obtained numerically from Eq. (2.14) as shown in Figure 3 ($\gamma = 0.96$). Here, $\partial F(\theta)/\partial\theta = 0$ at $\theta = \theta_{n_0}$, $n = 1,2, \ldots$ θ_{n_1} is defined by $F(\theta_{n_1}) = F(\theta_{n_0})$. For $\gamma = 0.96$, one has $\theta_{10} = 1.429$, $\theta_{n_0} = \theta_{10} + (n-1)\pi$; $\theta_{11} = 1.859$, $\theta_{n_1} = \theta_{11} + (n-1)\pi$. For $\theta_m \in [0,\theta_{10}]$ or $(\theta_{n_1}, \theta_{n+10})$, $u > 0$ for all $\theta \in [0, \theta_m)$. It is then possible to integrate Eq. (2.13) to obtain, in principle, $\theta = \theta(\xi)$ and hence $\theta_m = \theta_m(R)$. On the other hand, for $\theta_m \in [\theta_{n_0}, \theta_{n_1}]$, $u < 0$ for some θ, in contradiction to the requirement of $u(\equiv P^2/2) > 0$; Eq. (2.13) is insoluble. In other words, θ_m cannot be in $[\theta_{n_0}, \theta_{n_1}]$. The above analysis on the range of θ_m is independent of R and D [since $F(\theta)$ does not depend on R and D].

For each R, there may exist multiple solutions of θ_m. Indeed, Eq. (2.12) with Eq. (2.6) is solved numerically[12] for $\theta_m = \theta_m(R)$ in the range of $0 \leq R < 130$ (corresponding to the experiments of References 1 and 2). In the calculations, $K = 7.45 \times 10^{-7}$ dyn, $\gamma = 0.96$, $\gamma_2 = -0.8P$ are assumed.[15] Figure 4 shows a typical result. The existence of multiple values of θ_m for large R and the exclusion of θ_m in $[\theta_{10}, \theta_{11}]$ are evident.

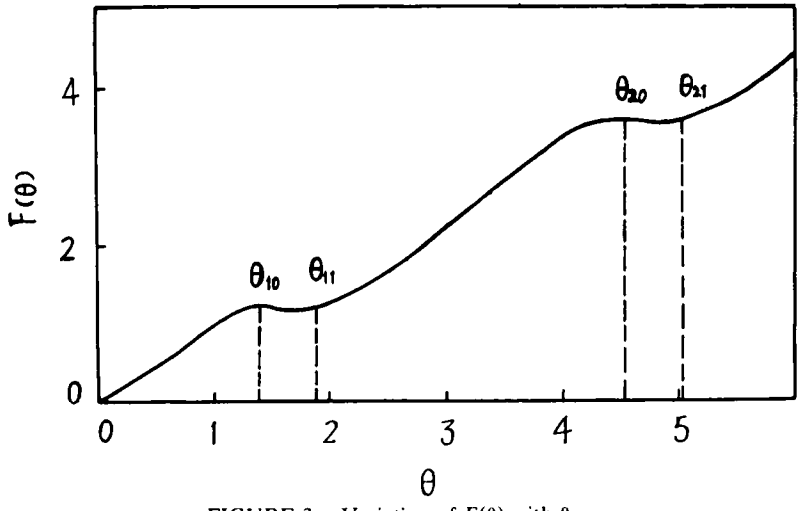

FIGURE 3. Variation of $F(\theta)$ with θ.

Numerical solutions

Equations (2.10) and (2.6) were solved numerically[12] for $R < 10$. In this range of R, from Figure 4, there exists only one branch of θ_m [and hence one possible solution of Eq. (2.10)]. Figure 5 represents a typical result for $0 \leqslant \theta_m < \theta_{10}$. θ_m defined previously as the value of θ at which $\partial\theta/\partial\xi = 0$ is also the maximum of θ in this case. The curve θ vs. ξ is symmetric under $\xi \rightarrow -\xi$. In this calculation, the values [15] $K_3 = 7.45 \times 10^{-7}$ dyn, $c = 0.85$, $b = 0.295$, $\gamma = 0.96$, $\gamma_2 = -0.8\,P$ for MBBA are assumed.

Small-angle approximation

For comparison, the case of small angle, $\theta << 1$, is considered. To second order in θ, Eq. (2.10) becomes

$$\frac{1}{D^2}\left[1 + (c - 1)\theta^2\right]\frac{d^2\theta}{d\xi^2} + \frac{c}{D^2}\,\theta\left(\frac{d\theta}{d\xi}\right)^2 - \frac{b}{R^2}\,\theta + R(1 + \gamma - 2\theta^2) = 0 \quad (2.16)$$

For $R < 12$ and the parameters used in Figure 5, numerical solutions of Eq. (2.16) are very close to that of Eq. (2.10) and are indistin-

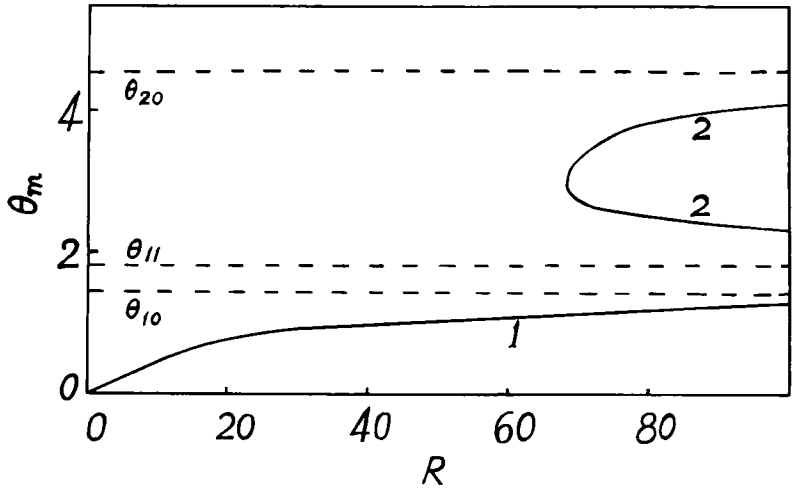

FIGURE 4. Multiple solutions of θ_m as function of R. $\omega_0 = 8.36 \times 10^{-4} s^{-1}$, $d = 150\ \mu m$.

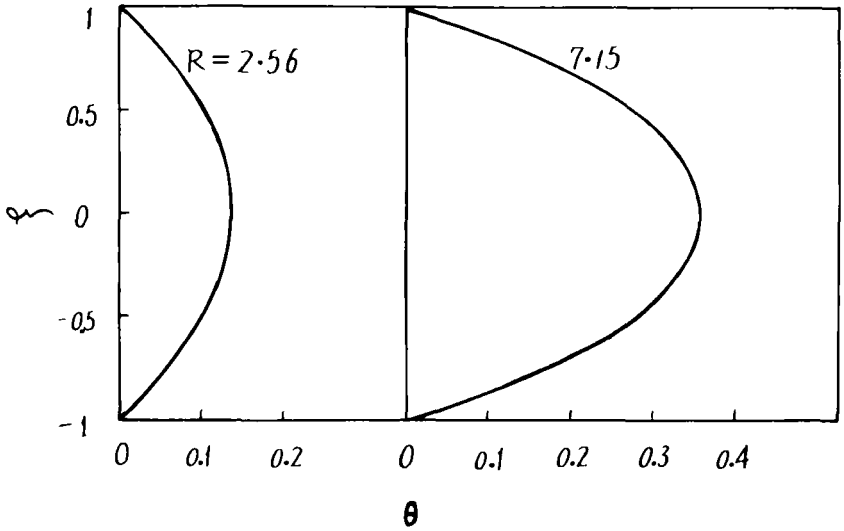

FIGURE 5. Calculated θ vs. ξ for R = 2.56 and 7.15, respectively. $\omega_0 = 8.36 \times 10^{-4} s^{-1}$, d = 150 μm. Eq. (2.10) is used.

guishable in the scales of Figure 5. In fact, the results show that $0 \leqslant \theta_m < 0.4$, indicating that the small-angle approximation is applicable in this region of R.

III. OPTICAL PATTERNS

For monochromatic light of wavelength λ_0 through crossed polarizers with polarization direction at 45° with the director plane, the transmitted light intensity is given by[16,17]

$$I = I_0 \sin^2\psi \tag{3.1}$$

where

$$\psi = \frac{\pi d}{2\lambda_0} \int_{-1}^{1} (n_e - n_0) d\xi \tag{3.2}$$

and

$$n_e - n_0 = n_0 [(1 - \alpha \sin^2\theta)^{-1/2} - 1] \tag{3.3}$$

$$\alpha \equiv 1 - (n_0/n_e)^2 \tag{3.4}$$

The numerical results for $\theta(\xi)$ from Model B of Section II are used in Eq. (3.3). The calculated [12] I/I_0 vs. R curve varies between zero and unity. The density of bright lines increases with increasing ω_0 for fixed d; it decreases with decreasing d for fixed ω_0. These bright lines correspond to those observed in the four quadrants in each photograph of interference patterns of References 1 and 2. The bright lines may be numbered beginning with $m = 1$ nearest to the center (the center itself is dark). [Note that m here has nothing to do with the subscript in θ_m used in Eq. (2.15). In Reference 1, m is used to number the dark lines instead.] For a given nematic, m depends on R and D.

In Table I, positions of the bright lines from numerical solutions of I/I_0 vs. R are presented. In the calculations, $n_e = 1.787$, $n_0 = 1.555$ and $\lambda_0 = 5460$ Å are assumed.[1] In References 1 and 2, the absolute scale of length is not given. For our purpose, this problem is solved by matching our calculated value of $R = 2.52$ for $m = 1$ in the case of $\omega_0 = 4.18 \times 10^{-4}\, s^{-1}$, $d = 194$ μm with the experimental position of the first bright ring of Reference 1 (see the third group of data in Table I). In the calculations presented in the rows

TABLE I.

Positions of bright rings in optical patterns. $m = i$ represents the i-th bright ring starting from the center. The numbers in rows represent R, the distance from center.

$\omega_0(10^{-4}s^{-1})$	d(μm)	$m = 1$	2	3	4	5	6	7
4.18	94	EXPT[a] 10.46						
		TH1[b] 9.60						
		TH2[c] 9.55						
		TH3[d] 9.50						
2.09	194	EXPT[a] 3.99	7.20	9.30	11.42			
		TH1 4.02	7.07	9.22	11.07			
		TH2 4.04	7.08	9.20	11.09			
		TH3 3.95	7.00	9.15	10.77			
4.18	194	EXPT[a] 2.52	4.49	5.85	7.08	7.99	9.04	
		TH1 2.52	4.43	5.80	6.96	7.99	8.98	
		TH2 2.53	4.44	5.81	6.99	8.03	9.03	
		TH3 2.49	4.52	5.88	6.78	7.69	8.59	
8.36	150	EXPT[e] 2.50	4.55	5.95	7.21	8.30	9.40	10.66
		TH1 2.55	4.50	5.92	7.14	8.26	9.33	10.34
		TH2 2.55	4.50	5.97	7.15	8.29	9.39	10.43
		TH3 2.48	4.44	5.90	6.98	8.07	8.69	9.62

[a]Experimental data from Reference 1.
[b]Theoretical result from Eq. (2.10).
[c]Theoretical result from Eq. (2.11).
[d]Theoretical result from Eqs. (4.4) and (4.5).
[e]Experimental data from Reference 2.

of TH1, TH2 and TH3, the same values of K_3, c, b, γ and γ_2 as in Figure 5 are used. TH1 represents the calculated results from Eqs. (2.10) and (3.1); TH2 those from Eqs. (2.16) and (3.1). As seen from Table I, as expected, these two results (the former does not use small-angle approximation; the latter does) do not differ too much from each other for $R < 10$. For $R > 10$, there are larger discrepancies between theory (not shown here) and experiments.[1,2]

For comparison, calculations from corrected Wahl-Fischer theory [Eq. (4.4) and Eq. (4.5)] are presented as TH3 in Table I (see Section IV).

The integer m, by definition, is given by $\psi = m\,\pi(I = I_0)$ or,

$$m = \frac{dn_0}{2\lambda_0}\int_{-1}^{1} d\xi[(1 - \alpha \sin^2\theta)^{-1/2} - 1] \tag{3.5}$$

When the calculated function $\theta = \theta(\xi;R)$ [R appears as parameters in Eqs. (2.10), (2.11) and (2.16)] is substituted into Eq. (3.5), we obtain $m = m(R)$ as a continuous function of R. Only those m with integer values represent the positions of the bright rings. By its definition, integer m is also the total number of bright rings within a distance of R from the center, which can be counted from the observed[1,2] optical patterns.

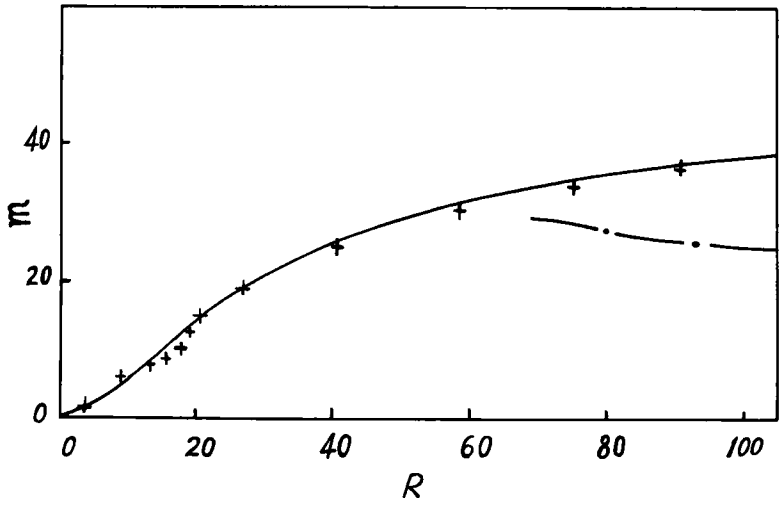

FIGURE 6. Calculated m vs. R. m is the order of interference defined by Eq. (3.5). The solid and dotted lines correspond to the first and second branch of solutions of Eq. (2.11), respectively. The crosses are experimental points read from Reference 2. ω_0 and d are the same as in Figure 4.

In Figure 6, the solid line represents a typical calculated m vs. R curve when the first-branch solution (see Figure 4) of Eq. (2.11) (parameters same as in Figure 4) is put into Eq. (3.5). The crosses are read from the experiments of Reference 2. Within the experimental range of $R < 130$, theory and experiment are consistent with each other. For $10 < R < 20$, deviation of theory from experiment is more obvious. This is the region in which the highest ring density (or minimum ring distance) appears.[2] It corresponds to a relatively rapid variation of θ with R so that our Model B is insufficient and Eq. (2.5) has to be used.

In Figure 6, the dotted line represents the result from the second-branch solution of Eq. (2.11). It begins at $R \sim 68$. Here, m should be understood as the order of interference as defined by Eq. (3.5).

Experiments[1,2] are consistent with the assumption that the first-branch solution is the physical one. The above conclusions are not altered when Eq. (2.10) is used in place of Eq. (2.11).

IV. COMPARISON WITH WAHL AND FISCHER

The theory of Wahl and Fischer[1] is based on the following basic assumptions:

(i) Rotation of the nematic is ignored. The director motion is treated as an one-dimensional uniform shear in the $(\hat{\varphi},\hat{z})$ plane (instead of a two-dimensional torsional shear as in our Section II) as described in Eq. (I1) [meaning Eq. (1) of Reference 1].
(ii) Near $r = 0$, θ is small.
(iii) θ is approximated by

$$\theta = \theta_2(r)(1 - \xi^2) + \theta_4(r)\xi^2(1 - \xi^2) \tag{4.1}$$

with $\theta_4/\theta_4 \equiv \epsilon << 1$.

Corrected results

Within these assumptions, the derivations in Reference 1 still contain a few errors. After corrections, Eq. (I4) should read

$$\overline{n_e - n_0} = \tfrac{1}{2}n_0\alpha \int_0^1 \left[\theta^2 - \left(\frac{1}{3} - \frac{3}{4}\alpha\right)\theta^4\right] d\xi \tag{4.2}$$

which has been pointed out in Reference 4. Eq. (I6) should read

$$\xi^2 = 1 - (\theta/\theta_2)(1 - \epsilon + \epsilon^2) - (\theta/\theta_2)^2(\epsilon - 3\epsilon^2) \tag{4.3}$$

Consequently, Eq. (I7) should read

$$\overline{n_e - n_0} = \frac{n_0}{2}\left[\left(\frac{8}{15} + \frac{16}{105}\epsilon\right)\theta_2^2 - \left(\frac{1}{3} - \frac{3}{4}\alpha\right)\left(\frac{384}{945} + \frac{512}{3465}\epsilon\right)\theta_2^4\right] \quad (4.4)$$

When Eq. (4.3) is put into Eq. (I1), one has

$$\theta_2 = \beta/(1 + 5\epsilon) \quad (4.5)$$

$$\theta_4 = \overline{K}\beta^3/(13\overline{K}\beta^2 - 3) \quad (4.6)$$

where

$$\epsilon = -\frac{1}{3}\overline{K}\beta^2\left(1 + \frac{8}{3}\overline{K}\beta^2\right)$$

$$\beta = \frac{\lambda_2 - \lambda_1}{16K_3}(\omega_0 rd)$$

$$\overline{K} \equiv (K_1 - K_3)/K_3 \quad (4.7)$$

$$\lambda_2 \equiv -\gamma_2,\ \lambda_1 \equiv -\gamma_1$$

The ϵ equation in Eq. (4.7) replaces Eq. (I10). Equation (I13) should be

$$a_4 = (5/7)(\lambda_0 a_2^2/n_e\alpha)[17(K_1 - K_3)/K_3 - (4/3 - 3\alpha)] \quad (4.8)$$

The notations not defined here are those in Reference 1.

In Reference 1, for MBBA, $n_0 = 1.555$, $n_e = 1.787$, $\lambda_0 = 5460$ Å, $a_2 = (16.4 \pm 0.2) \times 10^{23}\, m^{-5}\, s^2$, $a_4 = -(1.6 \pm 0.1) \times 10^{42}\, m^{-9}\, s^4$ are obtained. When these same numbers are put into Eq. (4.8), we obtain

$$K_1/K_3 = 0.813 \quad (4.9)$$

instead of $K_1/K_3 = 0.85 \pm 0.04$ as in Reference 1.

Equation (3.2) may be rewritten as

$$\psi = (\pi/\lambda_0)(\overline{n_e - n_0})d \quad (4.10)$$

Combining Eqs. (3.1), (4.4), (4.5), (4.7) and (4.10) one obtains I/I_0

vs. r by numerical method. $\gamma_2 = -0.8\ P$, $\gamma_1 = 0.768\ P$, $K_3 = 7.45 \times 10^{-7}$ dyn, $\overline{K} = -0.15$ (from Reference 15) and n_e, n_0, λ_0 from Reference 1 quoted above are adopted in the calculation. The positions of the bright lines expressed in R are presented as TH3 in Table I. As the optical pattern is concerned, this theory is consistent with experiment for $R < 6$. This range is almost half of ours in Section III.

It should be pointed out that the corrections in Eqs. (4.2) to (4.8) are in the order of β^4 and are relatively small in magnitude. In fact, we have repeated the calculations using the original (erroneous) equations of Reference 1; the difference appears in the third decimal point in comparison with TH3. Note that in Reference 1, there is neither calculation of the light intensity nor anything similar to our Table I or Figure 6.

Difference in director distribution

Although both Eqs. (2.10) and (I1) are one-dimensional and both assume $\partial\theta/\partial r = \partial^2\theta/\partial r^2 = 0$, they are based on different physical assumptions [see (i) above] and are quite different from each other. This may be seen more clearly in the one-constant approximation, in which the $(d\theta/d\xi)^2$ term vanishes in Eq. (I1) but not in Eq. (2.10) [i.e. Eq. (2.11)]. From our calculations, we know that this term does affect the director distribution.

In comparing $\theta(\xi)$ from Eq. (2.10) and Eq. (4.1), we see that $\theta_m[= \theta(\xi = 0)]$ from the former is smaller than that (i.e. θ_2) from the latter. For $R < 1$, because of the R^{-2} term, θ_m from Eq. (2.10) increases with R more slowly than θ_2 which increases linearly with R [see Eqs. (4.5) and (4.7), and Figures 9 and 10 of Reference 12]. A typical contrast of θ vs. ξ for different R from Eq. (2.10) and Eq. (4.1), respectively, is presented in Figure 7.

Error estimation

Our results on the locations of bright lines (m vs. R, see Table I) differs from experimental data by 0.3% while those of Wahl and Fischer[1] (after correction) is almost 4%. Our theory, Eq. (2.10), is obviously more close to experiments in this aspect.

In Reference 1, K_1/K_3 is deduced from a comparison between the approximate linear curve of $(m/d)/(vd)^2$ vs. $(vd)^2$ (where $v \equiv \omega_0 r$) and experimental results (see Figure 6 of Reference 1). There are two types of errors involved: (a) those coming from the deviation of

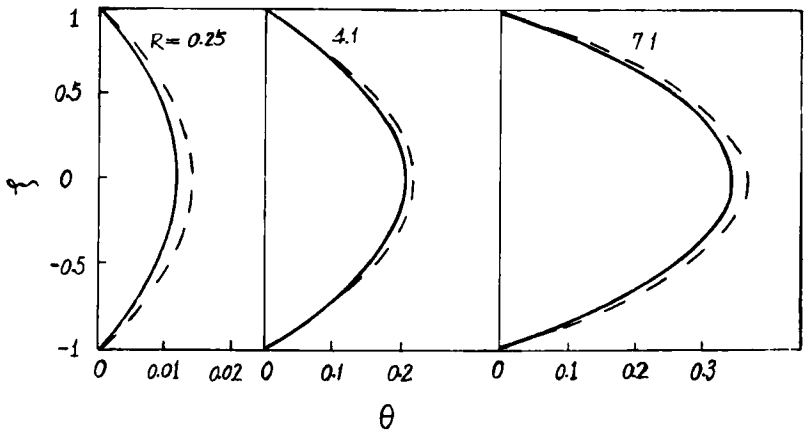

FIGURE 7. Comparison between calculated $\theta(\xi)$ from Eq. (2.10) (the solid lines) and Eq. (4.1) (the broken lines), respectively. ω_0 and d the same as in Figure 5. R = 0.25, 4.1, 7.1.

the experimental points from this curve, (b) those due to the basic assumptions [(i)–(iii)] and the different steps of approximations in the derivations. Reference 1 ignores type (b) completely and gives an error of 4.7% for K_1/K_3.

We now proceed to analyse type (b), taking the $\omega_0 = 8.36 \times 10^{-4} s^{-1}$, $d = 150$ μm case[2] as an example. In Figure 6 of Reference 1, the largest $(vd)^2$ value corresponds to a $R = 7.9$ which exceeds already the range of validity of the theory used ($R < 6$, see TH3 in Table I). At this R, θ_m of this theory differs from our result (which is more accurate) by already 7.1% (see Figure 7). This error due to the approximate nature of $(m/d)(vd)^2$ is already greater than that[1] quoted for K_1/K_3 (4.7%). If a smaller range of $(vd)^2$ from the origin in Figure 6 of Reference 1 is used, type (b) error may be reduced, but then, since the deviation of experimental points from the straight line is larger for $(vd)^2$ near zero, type (a) error will increase, rendering this strategy unpractical.

V. DISCUSSION

1. The director equation of motion describing the torsional shear flow, Eq. (2.3) or (2.5), is two-dimensional in nature. For a thick cell in which the z-variation may be ignored, Model A described by

the one-dimensional nonlinear ordinary differential equation

$$b\frac{d^2\theta}{dR^2} + \frac{1}{R}(b + \sin^2\theta)\frac{d\theta}{dR} - \frac{b}{2R^2}\sin 2\theta$$

$$- \frac{2(1-b)}{R^2}\sin^3\theta\cos\theta + R(\gamma + \cos 2\theta) = 0 \quad (5.1)$$

may be used. For a thin cell, as in the (steady-state) experiments of Wahl and Fischer,[1,2] the other one-dimensional Model B of Eq. (2.10) resulted from ignoring the r-variation is more appropriate.

2. As shown in Section III, our Model B is able to describe the position of the bright rings in the optical patterns for $R < 10$ and the total number of bright rings within R for $R < 130$ (these numbers are for MBBA). Inspite of these successes, our Model B, as well as the uncorrected or corrected theory of Wahl-Fischer in Section IV, fails to account for the existence of highest ring density (observed in some of the experimental photographs[1]). The failure is not difficult to understand. Rings of small separations correspond to a region in which θ varies rapidly with R, so that the approximation $\partial\theta/\partial R = 0$, used in both our Model B and the theory of Reference 1, is no longer valid. It therefore points to the need to solve the two-dimensional Eq. (2.5) if a full quantitative account of the experiments[1,2] is desired.

3. The Wahl-Fischer theory[1] is highly idealistic in ignoring completely the rotation of the material. Its equation, Eq. (I1), is quite different from our Model B, Eq. (2.10). Even when corrected, its validity range of R is about half that of our Model B (see Section IV). The error involved is larger than that indicated in Reference 1.

Accepting the limitations of our Model B, it will be nice to have analytic expressions so that it can be used to analyse the data and let one deduce K_1/K_3, say, in an easy way. In principle, this can be done by adopting the procedures used in Reference 1, including the use of Eq. (4.1) and the small-angle approximation (with appropriate corrections as presented in Section IV), but with Eq. (I1) replaced by our Eq. (2.10). This has acturally been done by us but we ended up with $K_1/K_3 = 0.187$ (in contrast to the usual value[15] of ~ 0.8). Since the small-angle approximation seems reasonable (see last paragraph in Section III, and TH1 and TH2 in Table I) for the range of R considered, it seems that it is Eq. (4.1) that is at fault (see Figure 7).

The fact that the approximation Eq. (4.1), when combined with

the less accurate Eq. (I1) in the fashion outlined in the first part of Section IV, does give $K_1/K_3 \sim 0.8$ may be somewhat fortuitous. We still believe that Eq. (4.1) or Eq. (I1), by itself, is an inadequate description of the torsional shear flow. This conclusion is further supported by the unsatisfactory results[12] obtained when we combine Eq. (4.1) with Eq. (2.5) to calculate θ vs. R.

4. In using the torsional shear experiments as a tool in determining the material constants, for a thin cell, the simplest procedure is to use the approach of Wahl and Fischer,[1] together with the corrections in our Section IV *and* using only those experimentally observed rings within a small R ($R < 6$ for MBBA) in the data analysis (which unfortunately is not the case in References 1–9).

To be more accurate, our Eq. (2.10) has to be used. One proceeds as before except that Eq. (I1) is now replaced by Eq. (2.10), if analytic expressions and simplicity are preferred. Otherwise, one has to solve Eq. (2.10) numerically and then $m(R)$ of Eq. (3.5) to fit the data. [Note that m vs. R (with integer m) is the only useful data from this type of experiment.[1,2]]

Ultimately, it is Eq. (2.5) that will provide the complete description (as long as ω_0 is not too large so that the director does not poke out of the tangent plane).

5. In all the numerical solutions performed in this paper, specific values of the material constants are prescribed. However, our conclusions are not affected by the specific choice.

In the presence of an external electric field E applied in the z-direction, the term $-\epsilon_a E^2 \cos\theta \sin\theta$ has to be added to the left-hand side of Eqs. (2.3) and (2.4). If E is replaced by magnetic field H, the $\epsilon_a E^2$ above should be replaced by $\chi_a H^2$. Time-dependent phenomena in torsional shear flow and related problems may be studied with Eq. (2.3).

Finally, let us emphasize that all the differential equations in this paper are valid for both homeotropic and planar nematics. The planar case can be discussed in exactly the same way.

Acknowledgments

We want to thank Xie Yuzhang and Shen Juelian for helpful discussions. One of us (L.L.) heartily thanks F. Fischer for reprints and useful correspondence.

References

1. J. Wahl and F. Fischer, *Mol. Cryst. Liq. Cryst.*, **22**, 359 (1973).
2. J. Wahl and F. Fischer, *Opt. Commun.*, **5**, 341 (1972).

3. K. Skarp and T. Carlsson, *Mol. Cryst. Liq. Cryst.*, **49**, 751 (1978).
4. J. Wahl, *Z. Narturf.*, **34a**, 818 (1979).
5. K. Skarp, T. Carlsson, S. T. Lagerwall and B. Stebler, *Mol. Cryst. Liq. Cryst.*, **66**, 199 (1981).
6. K. Skarp, T. Carlsson, I. Dhal, S. T. Lagerwall and B. Stebler, in Advances in Liquid crystal Research and Applications, ed. L. Bata (Pergamon Press, New York, 1980).
7. Th. Waltermann and F. Fischer, *Z. Naturf.*, **30a**, 519 (1975).
8. F. Fischer, J. Wahl and Th. Waltermann, in Berichte der Bunsen-Gesellschaft fur Physikalische Chemie (Verlag Chemie, Weihneim, 1974).
9. F. Fischer, *Z. Naturf.*, **31a**, 302 (1976).
10. Shu Changqing, Ph.D. Thesis, Institute of Physics, Chinese Academy of Sciences, Beijing, China (1984).
11. J. L. Ericksen, *Tran. Soc. Rheol.*, **5**, 23 (1961); F. M. Leslie, *Arch. Ration. Mech. Anal.*, **28**, 265 (1968).
12. He Gang, M. Sc. Thesis, Institute of Physics, Chinese Academy of Sciences, Beijing, China (1984).
13. L. Lam, *Z. Physik.*, **B27**, 349 (1977).
14. Lin Lei et al., *Phys. Rev. Lett.*, **49**, 1335 (1982); **52**, 2190 (1984).
15. P. G. deGennes, The Physics of Liquid Crystals (Clarendon Press, Oxford, 1974).
16. M. Born and E. Wolf, Principle of Optics (Pergamon Press, New York, 1964).
17. Lin Lei and Shu Changqing, *Acta Physica Sinica*, **33**, 165 (1984) [English translation to appear in Chinese Phys. (USA)].